Journal of Power Sources 216 (2012) 395–399

Contents lists available at SciVerse ScienceDirect

Journal of Power Sources

journal homepage: www.elsevier.com/locate/jpowsour

Short communication

Hydrothermal-synthesized $Co(OH)_2$ nanocone arrays for supercapacitor application

F. Cao*, G.X. Pan, P.S. Tang, H.F. Chen

Department of Chemistry, Huzhou Teachers College, Huzhou 313000, China

HIGHLIGHTS

- β-$Co(OH)_2$ nanocone arrays are prepared by a hydrothermal synthesis method.
- β-$Co(OH)_2$ nanocone arrays with high capacitance for supercapacitors application.
- 1D nanocone arrays structure keeps structure stable with good strain accommodation.

ARTICLE INFO

Article history:
Received 7 March 2012
Received in revised form
9 April 2012
Accepted 25 May 2012
Available online 1 June 2012

Keywords:
Cobalt hydroxide
Nanowire arrays
Supercapacitor
Porous film

ABSTRACT

$Co(OH)_2$ nanocone arrays are prepared by a facile hydrothermal synthesis method. The $Co(OH)_2$ nanocones are single crystalline in nature and have an average diameter of about 200 nm. The pseudocapacitive behavior of the $Co(OH)_2$ nanocone arrays is investigated by cyclic voltammograms (CV) and galvanostatic charge–discharge tests in 2 M KOH. As cathode for supercapacitor, the $Co(OH)_2$ nanocone arrays exhibit a capacitance of 562 F g^{-1} at 2 A g^{-1} as well as rather good cycling stability. The enhanced supercapacitor performances are due to the porous array architecture providing fast ion and electron transfer, large reaction surface area and good strain accommodation.

1. Introduction

Supercapacitor has attracted great attention due to high power performance, fast recharge capability, long cycle life, and low maintenance cost [1–3]. In the past decade, lots of research has been dedicated to investigating pseudocapacitive materials such as hydroxides [4,5], oxides [6,7], and polymers [8,9], which produce increased specific capacitances and high energy densities. In recent years, Cobalt species materials such as $Co(OH)_2$, CoOOH, and Co_3O_4 have attracted great attention due to their excellent electrochemical reversibility and cycle life and high capacitances [10–12]. Among these available pseudocapacitive candidates, $Co(OH)_2$ is considered to be one of the most attractive materials owing to its high specific capacitance (theoretical specific capacitance $\geq$ 2600 F g^{-1}) [12–14], well-defined electrochemical redox activity and low cost.

Pseudocapacitive process is determined by the kinetics feature of the electrode [4]. Over recent years, self-supported one-dimensional (1D) array architecture (nanorods, nanotubes and nanocones, etc.) directly grown on conductive substrates has been demonstrated to be an optimized architecture for boosting the pseudocapacitive performance due to its short and fast diffusion path for ions and electrons, resulting in reduced internal resistance and improved high-power capability [15–17]. Up to now, most of the research about pseudocapacitance of $Co(OH)_2$ heavily focus on two-dimensional $Co(OH)_2$ nanoflake arrays grown by electrodeposition methods [18–21], and there are only a few reports about self-supported 1D $Co(OH)_2$ arrays for supercapacitor application. Previously, Jiang et al. [22] and Yuan et al. [23] reported $Co(OH)_2$ nanowire arrays via hydrothermal synthesis methods and enhanced supercapacitor performance were obtained. In the present work, we report a self-supported single-crystalline β-$Co(OH)_2$ nanocone arrays prepared by a facile hydrothermal synthesis method and demonstrate the high-rate energy storage in supercapacitor application with high specific capacitance and quite good cycling stability.

2. Experimental

The $Co(OH)_2$ nanocone arrays were prepared by immersing clean nickel foam (a size of 3 × 6 cm^2) into the mixed solution of

* Corresponding author. Tel./fax: +86 572 232 1166.
E-mail address: caofenghz@126.com (F. Cao).

0378-7753/$ – see front matter © 2012 Elsevier B.V. All rights reserved.
doi:10.1016/j.jpowsour.2012.05.073

5 mmol $Co(NO_3)_2$, 10 mmol NH_4F, 15 ml of 28 wt.% ammonia solution and 20 ml of H_2O. The top side of nickel foam was protected from solution contamination by uniformly coating with a polytetrafluorethylene tape. The autoclave was sealed and maintained at 120 °C for 5 h for nanocone array growth. Finally, the sample was fetched out and rinsed with distilled water several times in order to remove the residual nanoparticle debris. The load weight of $Co(OH)_2$ nanocone arrays was about 3.5 mg cm^{-2}.

The morphology and structure of samples were characterized by X-ray diffraction (XRD, RIGAKU D/Max-2550 with Cu Kα radiation), field emission scanning electron microscopy (FESEM, FEI SIRION), high-resolution transmission electron microscopy (HRTEM, JEOL JEM-2010F). The surface area of the film power scratched from the substrate was determined by BET (Brunauer–Emmett–Teller) measurements using a NOVA-1000e surface area analyzer.

The electrochemical measurements were carried out in a three-electrode electrochemical cell containing 2 M KOH aqueous solution as the electrolyte. Cyclic voltammetry (CV) measurements were performed on a CHI660c electrochemical workstation. CV measurements were carried out at 25 °C, self-supported $Co(OH)_2$ nanocone arrays as the working electrode, Hg/HgO as reference electrode and a Pt foil as counter-electrode. The galvanostatic charge–discharge tests were conducted on a LAND battery program-control test system. The as-prepared electrodes, together with a nickel mesh counter electrode and an Hg/HgO reference electrode were tested in a three-compartment system.

3. Results and discussion

The as-deposited film is uniform in appearance and exhibits red in color. XRD characterization shows that the as-grown film is exclusively brucite β-$Co(OH)_2$ phase (Fig. 1). Except for three representative peaks from nickel foam substrate, other diffraction peaks are well indexed to β-$Co(OH)_2$ (JCPDS 30-0443). SEM and TEM images of the β-$Co(OH)_2$ nanocone arrays are presented in Fig. 2. The skeletons of the nickel foam are uniformly covered by the nanocones with diameters of about 200 nm, which grow densely and almost vertically to the substrate (Fig. 2a and b). Further insight into the microstructure of the nanocone is obtained by TEM. Typical TEM image confirms that the average diameter of an individual β-$Co(OH)_2$ nanocone is about 200 nm (Fig. 2c). According to the pattern of selected area electronic diffraction (SAED) (Fig. 2c), the β-$Co(OH)_2$ nanocone is single crystalline in nature with a growth direction along (001), which is consistent with the XRD result. It is believed that this porous 1D array feature is helpful to the enhancement of electrochemical properties because it would lead to fast ion/electron transfer, sufficient contact between active materials and electrolyte, and enhanced flexibility.

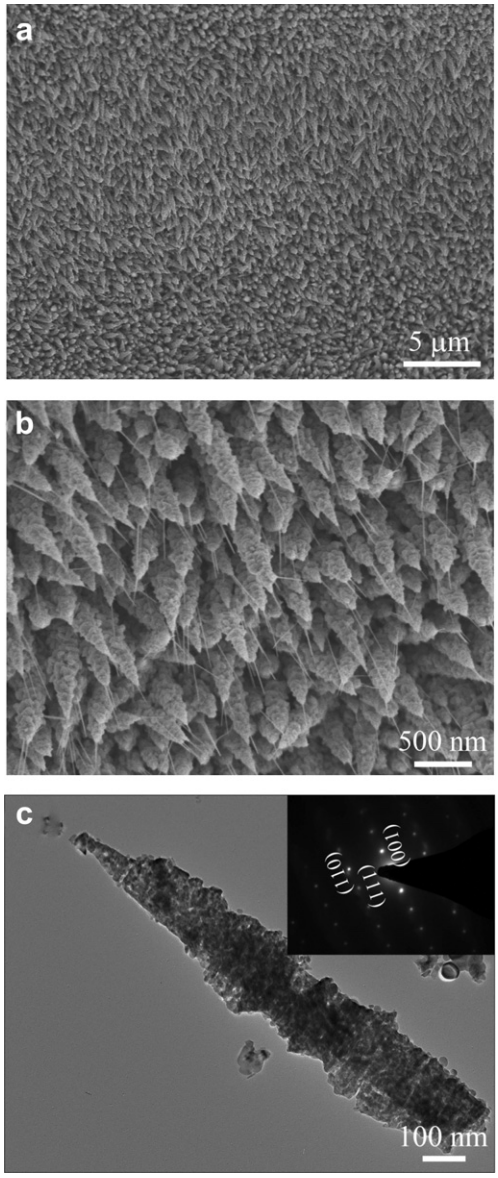

Fig. 2. (a), (b) SEM images of the β-$Co(OH)_2$ nanocone arrays grown on nickel foam; (c) TEM image of the β-$Co(OH)_2$ nanocone (SAED pattern presented in inset).

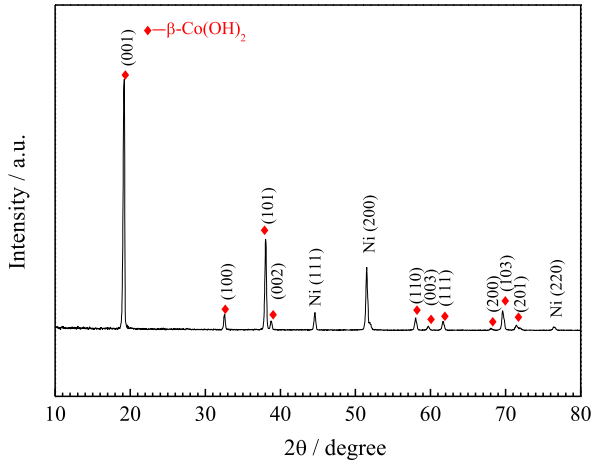

Fig. 1. XRD pattern of the β-$Co(OH)_2$ nanocone arrays grown on nickel foam.

The pseudocapacitive behavior of the β-$Co(OH)_2$ nanocone arrays is investigated by cyclic voltammograms (CV) and galvanostatic charge–discharge tests in 2 M KOH. Fig. 3a and b shows the CV curves of the β-$Co(OH)_2$ nanocone arrays between at different scanning rates. Note that the CV curves consist of two pairs of strong redox couples P1/P4 and P2/P3, indicating that the capacitance characteristics are governed by Faradaic reactions, distinct from that of the electric double-layer capacitance, which would produce a CV curve close to an ideal rectangular shape. The redox couple P1/P4 is due to the change between $Co(OH)_2$ and CoOOH, which can be simply illustrated as follows [21,22].

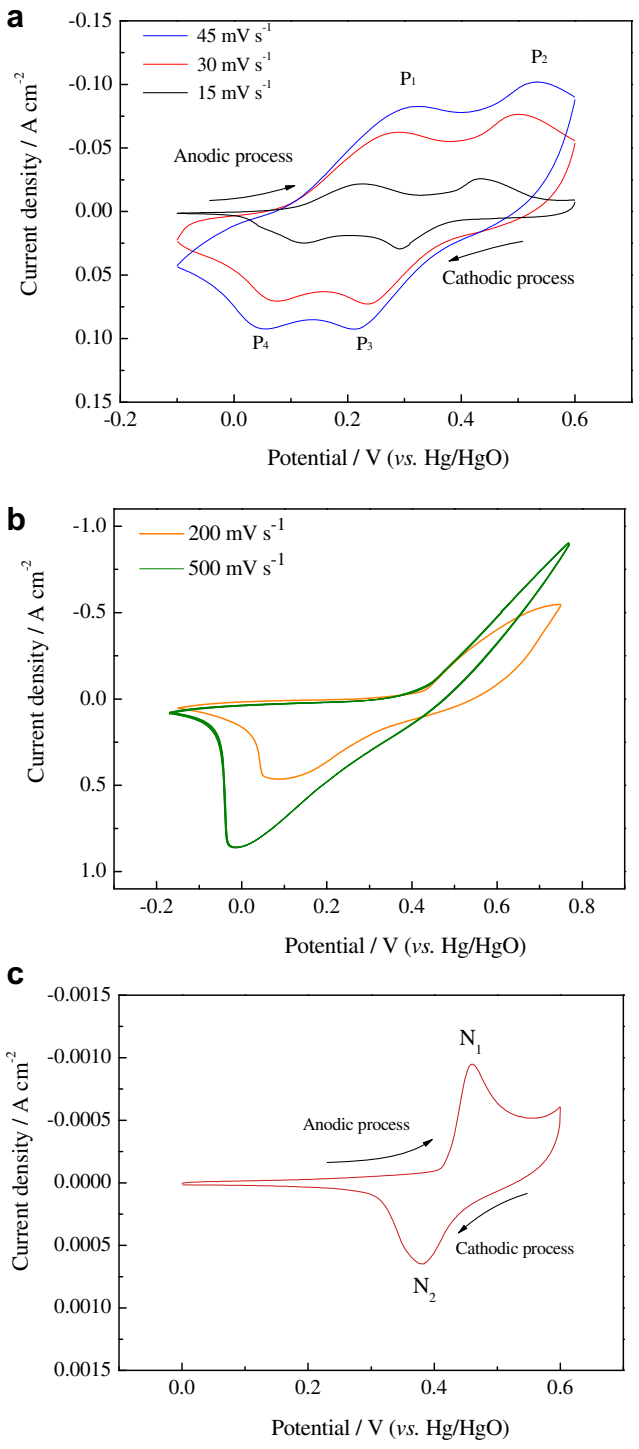

Fig. 3. Cyclic voltammograms of the (a), (b) β-$Co(OH)_2$ nanocone arrays at different scanning rate. (c) CV curve of the nickel foam at the scanning rate of 10 mV s^{-1}.

$$Co(OH)_2 + OH^- \leftrightarrow CoOOH + H_2O + e^- \quad (1)$$

The redox couple P2/P3 at higher potential is assigned to the conversion between CoOOH and CoO_2, illustrated as follows [21,22].

$$CoOOH + OH^- \leftrightarrow CoO_2 + H_2O + e^- \quad (2)$$

The CV behavior changes much as the scanning rate increases (Fig. 3a and b). The oxidation and reduction peaks shift continuously to higher and lower potentials respectively, leading to a larger potential separation between the oxidation and the reduction peak. Furthermore, two oxidation (P_1 and P_2) and reduction peaks (P_3 and P_4) merges with each other leaving one oxidation and reduction peaks at a scanning rate of 200 and

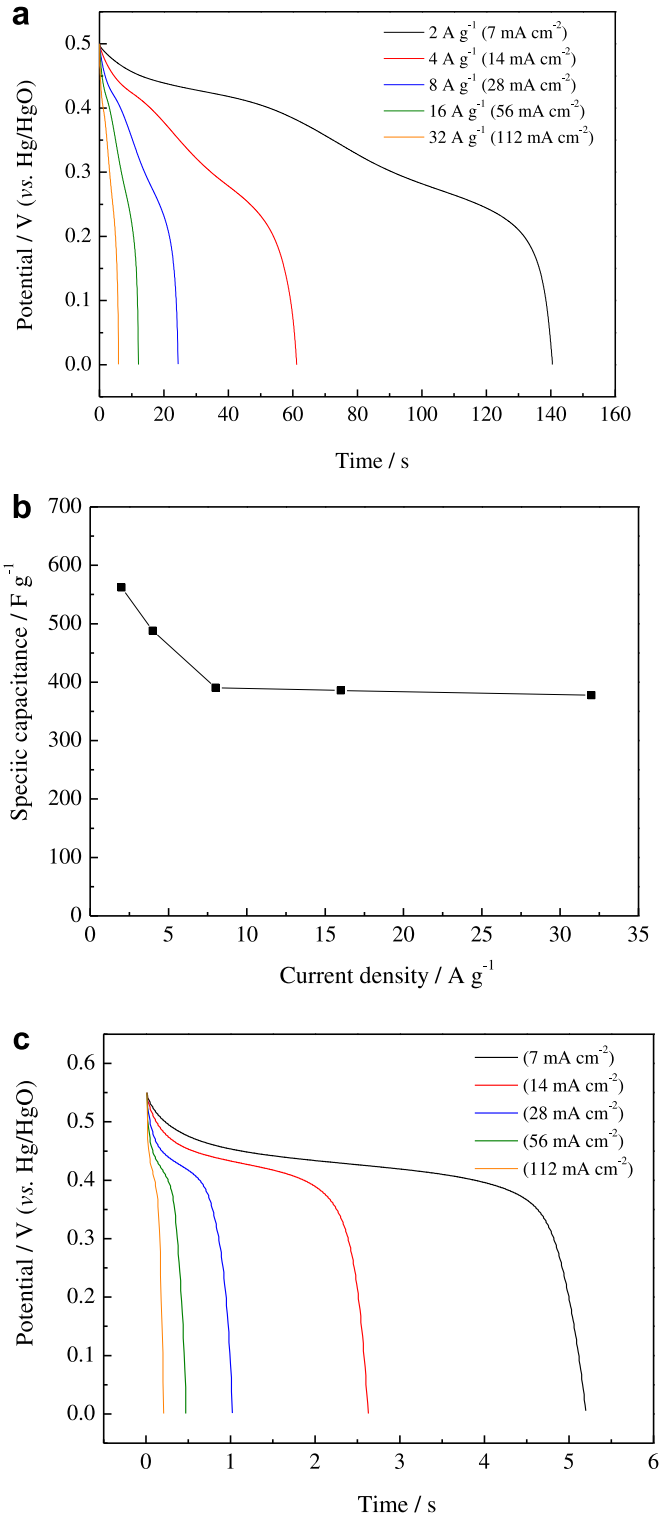

Fig. 4. (a) Discharge curves of the β-$Co(OH)_2$ nanocone arrays at different discharge current densities and (b) corresponding capacitances. (c) Discharge curves of the nickel foam at different discharge current densities.

500 mV s^{-1}, respectively. In addition, the nickel foam substrate also exhibits a redox process N_1/N_2 (Fig. 3c), which is due to the reversible reactions of Ni(II)/Ni(III) formed on the nickel surface, but its peak current intensities are much lower than those of the β-$Co(OH)_2$ nanocone arrays. Though the redox process N_1/N_2 will contributes to the specific capacitance of the films, its contribution is quite small less than 5%. High scanning rate corresponds to the high-rate charge–discharge process. Hence, the specific capacitance decreases when the scanning rate increases. Average specific capacitance values were calculated from the CV curves using the following equation:

$$C = \frac{\int I dt}{m\Delta V} \quad (3)$$

where I is the oxidation or reduction current, dt is the time differential, m and ΔV indicate the mass of the active electrode material and the voltage range of one sweep segment, respectively. The average specific capacitance of the β-$Co(OH)_2$ nanocone arrays is calculated to be 530 F g^{-1} at a scanning rate of 10 mV s^{-1} and 365 F g^{-1} at a higher scanning rate of 40 mV s^{-1}. In our case, the electrochemical reversibility is only fair but not quite good. Its electrochemical reversibility is worse than Co_3O_4 [13,24], and CoOOH [10] in the literature. However, the electrochemical reversibility of our $Co(OH)_2$ nanocone film is similar to those of $Co(OH)_2$ reported in the literature [23,25–27]. It is indicated that its relative poor electrochemical reversibility will cause worse high-rate capability, confirmed by the charge–discharge tests as below (Fig. 4).

Discharge curves of the β-$Co(OH)_2$ nanocone arrays and corresponding specific capacitances at various discharge current densities are shown in Fig. 4a and b. The specific capacitance was calculated according to the following equation:

$$C = \frac{I\Delta t}{M\Delta V} \quad (4)$$

where C (F g^{-1}) is the specific capacitance, I (mA) represents discharge current, and M (mg), ΔV (V) and Δt (s) designate mass of active materials, potential drop during discharge and total discharge time, respectively.

The supercapacitor properties are tested by galvanostatic charge–discharge at different current densities with 7 mA cm^{-2} (corresponding to 2 A g^{-1} based on mass of $Co(OH)_2$), 14 mA cm^{-2} (4 A g^{-1}), 28 mA cm^{-2} (8 A g^{-1}), 56 mA cm^{-2} (16 A g^{-1}), and 112 mA cm^{-2} (32 A g^{-1}), respectively. The pseudocapacitances are obtained by subtracting the discharge time of nickel foam to reduce the substrate effect to the lowest level. And as shown in Fig. 4c, the nickel foam only exhibits small capacitance with several discharge seconds. The β-$Co(OH)_2$ nanocone arrays exhibit a pseudocapacitance of 562 F g^{-1} at 2 A g^{-1}, 488 F g^{-1} at 4 A g^{-1}, 390 F g^{-1} at 8 A g^{-1}, 385 F g^{-1} at 16 A g^{-1} and 377 F g^{-1} at 32 A g^{-1}, respectively. These values are higher than those obtained from NiO nanowire arrays [28], and comparable to Co_3O_4 nanowire arrays [29] and $Co(OH)_2$ nanowire arrays reported by Jiang et al. [22] and Yuan et al. [23], but much lower than those porous electrodeposited α-$Co(OH)_2$ nanoflakes films [18].

Fig. 5a and b presents the cycle characteristics of the β-$Co(OH)_2$ nanocone arrays at a current density of 2 A g^{-1}. In order to measure the cycle life of specific capacitance of the β-$Co(OH)_2$ nanocone arrays more concisely, we recorded the discharge electric quantity (Q) of the β-$Co(OH)_2$ nanocone arrays and nickel foam (Fig. 5a). Notice that the discharge electric quantity of the nickel foam

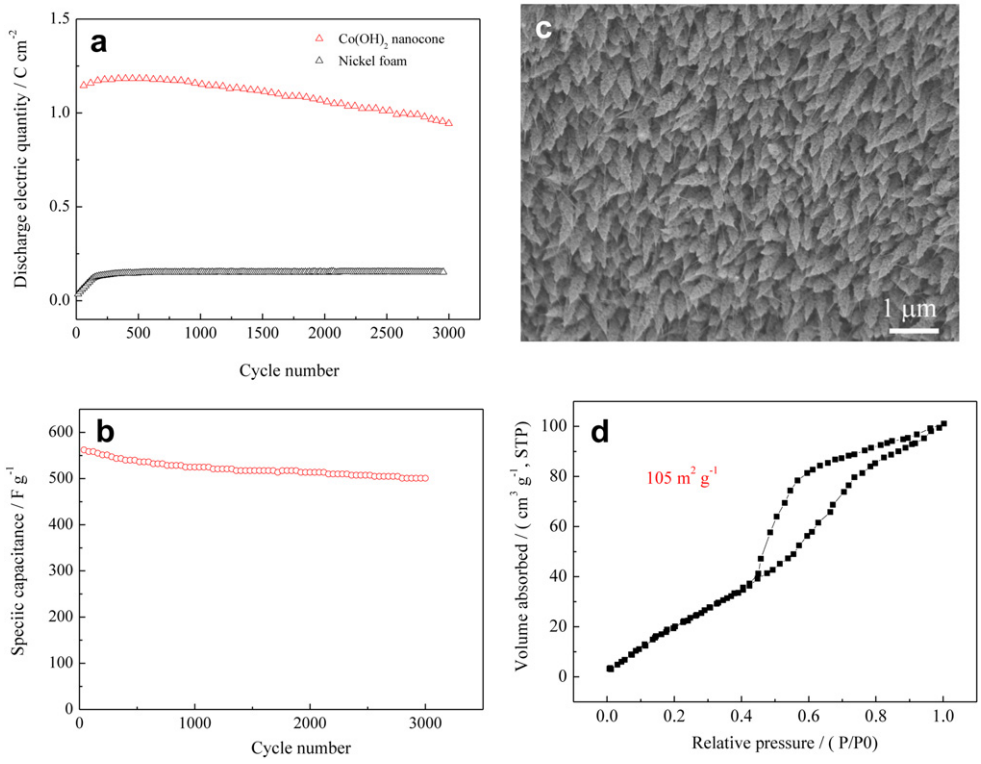

Fig. 5. (a) Cycling performance of discharge electric quantity of the β-$Co(OH)_2$ nanocone arrays and nickel foam at 7 mA cm^{-2} (corresponding to 2 A g^{-1} based on mass of $Co(OH)_2$); (b) cycling performance of specific capacitance of the β-$Co(OH)_2$ nanocone arrays at 7 mA cm^{-2} (2 A g^{-1}); (c) SEM images of the fully discharged β-$Co(OH)_2$ nanocone arrays after 3000 cycles; (d) BET measurement of the β-$Co(OH)_2$ nanocone arrays.

increases up to about 500 cycles, the remains practically constant (Fig. 5a). It is indicated that the capacitance contribution from the nickel foam increases up to about 500 cycles and keeps stable. The specific capacitance of the β-$Co(OH)_2$ nanocone arrays during cycle was calculated according to the equation:

$$C = \frac{Q}{V} \tag{5}$$

where C is specific capacitance, and V is voltage across the electrodes, and Q is discharge electric quantity obtained by the β-$Co(OH)_2$ nanocone arrays minus nickel foam. Fig. 5b is the cycling performance of specific capacitance of the β-$Co(OH)_2$ nanocone arrays. Notice that the β-$Co(OH)_2$ nanocone arrays do not have an activation process, which is prevailing in oxides for supercapacitors [10,13]. The β-$Co(OH)_2$ nanocone arrays exhibit quite good pseudocapacitance retention with 501 F g^{-1} after 3000 cycles maintaining 88% of the maximum value. Fig. 5c shows the SEM image of the arrays after 3000 cycles. The β-$Co(OH)_2$ nanocone arrays keep the structure integrity, indicating that the 1D nanocone array structure is stable up to 3000 cycles leading to enhanced cycle life. The pretty good pseudocapacitive performance of the β-$Co(OH)_2$ nanocone arrays is mainly due to the 1D nanocone array architecture. The open space between neighboring nanocones allows for easy diffusion of electrolyte into the inner region of the electrode, resulting in reduced internal resistance and improved high-power performance. Each nanocone has its own contact with the substrate at the bottom. This can ensure every nanocone participates in the electrochemical reaction [30,31]. Using nanocone arrays also saves the tedious process of mixing active material with ancillary materials such as carbon black and polymer. Moreover, nanocones share the same advantages as other nanostructured electrodes that provide shorten diffusion paths for both electrons and ions, larger surface area (Fig. 5d) and more active sites for electrochemical reactions. These features are particularly helpful for high rate applications, resulting in rather good pseudocapacitive performance.

4. Conclusions

In summary, self-supported β-$Co(OH)_2$ nanocone arrays are prepared by a facile hydrothermal synthesis method and show single crystalline in nature. The β-$Co(OH)_2$ nanocone arrays exhibit rather good pseudocapacitive performance with high specific capacitance of 562 F g^{-1} at 2 A g^{-1} and good cycling stability. The enhanced electrochemical capacitive performance is mainly due to the high porosity and large surface area of the porous 1D array architecture. Additionally, the 1D array architecture is very stale leading to enhanced cycling stability.

References

[1] J.R. Miller, P. Simon, Science 321 (2008) 651.
[2] P. Simon, Y. Gogotsi, Nat. Mater. 7 (2008) 845.
[3] Y. Zhang, H. Feng, X.B. Wu, L.Z. Wang, A.Q. Zhang, T.C. Xia, H.C. Dong, X.F. Li, L.S. Zhang, Int. J. Hydrogen Energy 34 (2009) 4889.
[4] C. Liu, F. Li, L.P. Ma, H.M. Cheng, Adv. Mater. 22 (2010) E28.
[5] X.H. Xia, J.P. Tu, Y.Q. Zhang, Y.J. Mai, X.L. Wang, C.D. Gu, X.B. Zhao, J. Phys. Chem. C (2011) dx.doi.org/10.1021/jp208113j.
[6] Y.Y. Gao, S.L. Chen, D.X. Cao, G.L. Wang, J.L. Yin, J. Power Sources 195 (2010) 1757.
[7] A. Cross, A. Morel, A. Cormie, T. Hollenkamp, S. Donne, J. Power Sources 196 (2011) 7847.
[8] J.H. Huang, C.W. Chu, Electrochim. Acta 56 (2011) 7228.
[9] G.A. Snook, P. Kao, A.S. Best, J. Power Sources 196 (2011) 1.
[10] E. Hosono, S. Fujihara, I. Honma, M. Ichihara, H.S. Zhou, J. Power Sources 160 (2006) 764.
[11] T.Y. Wei, C.H. Chen, K.H. Chang, S.Y. Lu, C.C. Hu, Chem. Mater. 21 (2009) 3228.
[12] L. Cao, F. Xu, Y.Y. Liang, H.L. Li, Adv. Mater. 16 (2004) 1853.
[13] C.C. Hu, T.Y. Hsu, Electrochim. Acta 53 (2008) 2386.
[14] C. Lin, J.A. Ritter, B.N. Popov, J. Electrochem. Soc. 145 (1998) 4097.
[15] R. Liu, S.B. Lee, J. Am. Chem. Soc. 130 (2008) 2942.
[16] C.C. Hu, K.H. Chang, M.C. Lin, Y.T. Wu, Nano Lett. 6 (2006) 2690.
[17] G. Wang, L. Zhang, J. Zhang, Chem. Soc. Rev. (2011). doi:10.1039/c1cs15060j.
[18] W.J. Zhou, J. Zhang, T. Xue, D.D. Zhao, H.L. Li, J. Mater. Chem. 18 (2008) 905.
[19] C.Z. Yuan, L.R. Hou, D.K. Li, L.F. Shen, F. Zhang, X.G. Zhang, Electrochim. Acta 56 (2011) 6683.
[20] J.K. Chang, C.M. Wu, I.W. Sun, J. Mater. Chem. 20 (2010) 3729.
[21] C.M. Wu, C.Y. Fan, I.W. Sun, W.T. Tsai, J.K. Chang, J. Power Sources 196 (2011) 7828.
[22] J. Jiang, J.P. Liu, R.M. Ding, J.H. Zhu, Y.Y. Li, A.Z. Hu, X. Li, X.T. Huang, ACS Appl. Mater. Interfaces 3 (2011) 99.
[23] C.Z. Yuan, X.G. Zhang, L.R. Hou, L.F. Shen, D.K. Li, F. Zhang, C.G. Fan, J.M. Li, J. Mater. Chem. 20 (2010) 10809.
[24] C. Barbero, G.A. Planes, M.C. Miras, Electrochem. Commun. 3 (2001) 113.
[25] T. Zhao, H. Jiang, J. Ma, J. Power Sources 196 (2011) 860.
[26] Y.Y. Liang, S.J. Bao, H.L. Li, J. Solid State Electrochem. 11 (2007) 571.
[27] C.Y. Yan, H. Jiang, T. Zhao, C.Z. Li, J. Ma, P.S. Lee, J. Mater. Chem. 21 (2011) 10482.
[28] H. Pang, Q.Y. Lu, Y.Z. Zhang, Y.C. Li, F. Gao, Nanoscale 2 (2010) 920.
[29] X.H. Xia, J.P. Tu, Y.J. Mai, X.L. Wang, C.D. Gu, X.B. Zhao, J. Mater. Chem. 21 (2011) 9319.
[30] X.H. Xia, J.P. Tu, X.L. Wang, C.D. Gu, X.B. Zhao, Chem. Commun. 47 (2011) 5786.
[31] X.H. Xia, J.P. Tu, X.L. Wang, C.D. Gu, X.B. Zhao, J. Mater. Chem. 21 (2011) 671.